Journal of Power Sources 248 (2014) 668–678

Contents lists available at ScienceDirect

Journal of Power Sources

journal homepage: www.elsevier.com/locate/jpowsour

Enhanced fuel cell hybrid electric vehicle power sharing method based on fuel cost and mass estimation

Khalil Maalej [a], Sousso Kelouwani [a,*], Kodjo Agbossou [b], Yves Dubé [a]

[a] Hydrogen Research Institute and the Department of Mechanical Engineering of Université du Québec à Trois-Rivières, Trois-Rivières, Québec G9A 5H7, Canada

[b] Hydrogen Research Institute and the Department of Electrical and Computer Engineering of Université du Québec à Trois-Rivières, Trois-Rivières, Québec, G9A 5H7, Canada

HIGHLIGHTS

- A method for selecting an optimal driving cycle knowing a trip road.
- A method for adaptive energy management using online vehicle mass estimation.
- A comparative study demonstrating the effectiveness of the adaptive method.

ARTICLE INFO

Article history:
Received 27 June 2013
Received in revised form
27 September 2013
Accepted 29 September 2013
Available online 10 October 2013

Keywords:
Electric vehicle
Energy efficiency
Energy management
Fuel cell
Nonlinear optimal control
Vehicle dynamics

ABSTRACT

In this paper, we investigate an adaptive energy management and power splitting system for a fuel cell hybrid electric vehicle. The battery pack is the main power source whereas the fuel cell is considered as a range extender that cannot sustain alone the vehicle traction power. In addition, the fuel cell contributes to reduce the battery pack degradation by limiting its depth-of-discharge (DoD). This energy management system is based on a two layer architecture in which the upper layer computes the anticipated end-of-trip DoD using online mass estimation. The lower layer is designed to split the driver power demand by minimizing a cost function which includes the hydrogen/electricity cost ratio. Therefore, the best trade-off between reducing battery pack degradation and using cost effective energy is provided. Furthermore, the system allows the fuel cell to operate at its maximum efficiency. Comparative study results indicate that using online mass estimation improves the overall fuel consumption efficiency whilst contributing at the same time to DoD reduction.

1. Introduction

Terrestrian vehicle powertrain electrification is a key step towards the reduction of the greenhouse gas emission sources [1]. However, the use of batteries as a power source for vehicles raises several challenges that must be addressed to make it competitive: limited operating range, long charging time, limited lifespan, etc. Vehicle source hybridization has been proposed as a practical way to increase fuel usage efficiency and to extend operating range [2]. Thus, plugin hybrid vehicles (PHEV) with gasoline internal-combustion engines as range extenders have been proposed by car makers and several of such vehicles are being deployed around the word: Chevrolet Volt of General Motor, Outlander PHEV of Mitsubishi, etc. However, it is noteworthy that gasoline used in these vehicles contributes to the greenhouse gas emission [3,4].

To completely remove any fossil energy on the vehicle, a clean-energy vector such as hydrogen attracts a lot of attention in research community [5]. Indeed, hydrogen has one of the highest energy densities per weight and can be used in fuel cell to produce electricity or burned in an internal combustion engine (ICE) to directly generate propulsion torque [6]. Some of PHEVs with hydrogen as energy vector have been proposed in the literature [7–9]. Fuel cell PHEV (FC-PHEV) has received more attention than hydrogen-based ICE.

The vehicle global fuel saving is thoroughly related to the power flow control between each energy source and the powertrain [10,11]. Several energy management and power sharing control systems for hybrid electric vehicles (HEV) as well as PHEV have been reported throughout the literature: rule-based methods

* Corresponding author.
E-mail addresses: Khalil.Maalej@uqtr.ca (K. Maalej), sousso.kelouwani@uqtr.ca, sousso.kelouwani@gmail.com (S. Kelouwani), kodjo.agbossou@uqtr.ca (K. Agbossou), yves.dube@uqtr.ca (Y. Dubé).

0378-7753/$ – see front matter © 2013 Elsevier B.V. All rights reserved.
http://dx.doi.org/10.1016/j.jpowsour.2013.09.127

[8,12], optimization methods [13–15], stochastic approaches and adaptive approaches [16,17]. These methods belong to the blended mode energy management systems. Most of these works assumed that the power demand from the vehicle driver is known. However, the driver often provides a control signal using the vehicle acceleration pedal. One way to determine the corresponding power demand is to use the vehicle longitudinal dynamics which considers that the mass and other physical parameters (rolling resistance coefficient, road grade, air density, vehicle frontal area, and aerodynamic drag coefficient) as known beforehand. Whilst some of these parameters can be assumed to be constant values, the vehicle mass as well as the road grade can change during the trip. In addition, most of the reported work assumed that the on-board energy sources have similar power range, and the energy cost is not directly taken into account. Having similar operating power range simplifies the design of the energy management system. Indeed, the well-known charge-depleting charge-sustaining method can be easily used: after the battery pack has been depleted, the secondary energy source can sustain the power demand so that at the end of the trip, the battery pack energy remains close to a given low value. In addition, in blended mode, the power demand needs to be estimated in order to properly use the secondary energy source to supplement the battery pack.

This paper investigated the energy management and the real-time power splitting problems of a serial topology FC-PHEV in which the battery pack is the primary and the most powerful energy source and the fuel cell is considered as a range extender (fewer powerful energy source). Therefore, the charge-depleting charge-sustaining method cannot be used since the fuel cell is unable to sustain the power demand. So, to maintain battery pack energy close to a prescribed minimum value at the end of a trip, the fuel cell operating sequence must be carefully designed. In addition, we assume that when the vehicle is stopped during a trip, the mass may change (change in the number of passengers in the vehicle, garbage trucks, delivery trucks and buses, etc.). Furthermore, it can be used for small vehicles that cannot support the weight of a great fuel cell (mass-power ratio).

The mass estimation in the context of hybrid electric vehicle energy management has not been fully addressed in the literature. It becomes a key step towards a good energy planning system, and its online estimate is challenging. Several mass and grade estimation methods reported throughout the literature can be classified in two categories [18]: event-based and averaging. Each of these categories could be further divided into two sub-category: simultaneous estimation of mass and grade, single estimation of mass using grade measurements. For these estimations, different vehicle dynamic models were used [18]: suspension dynamics [19], yaw dynamics [20], drive-train dynamics and longitudinal dynamics [21–23].

Event-based methods seek for driving conditions that provide sufficient excitation for mass or grade estimation: model predictive approach [24], use of grade estimation with GPS (Global Positioning System) to derive mass estimation [25] and supervisory control approaches [18].

Instead of seeking for events, the averaging method continuously monitors the vehicle dynamics in order to directly estimate the mass and grade online, using recursive least squares (RLS) [21,23,26,27] and Kalman's filter. Others reported methods can be seen in Refs. [22,28].

The proposed energy management system is based on a two-layer architecture in which the supervisor (high level of the architecture) is responsible for providing the global energy consumption profile when the vehicle mass is not constant and the anticipated battery depth-of-discharge (DoD). Given the global consumption profile, the lower level provides a locally optimal power sharing between the fuel cell and the battery pack by minimizing a cost function which includes the hydrogen and electricity price ratio.

The rest of the paper is organized into seven sections. The FC-PHEV description and its longitudinal model are presented in Sections 2 and 3, respectively. Based on this model, a new adaptive energy management system is described and discussed in Section 4. Section 5 is related to the design of the lower layer (power splitting method). The adaptive energy planning and the power splitting method validations are provided in Sections 6 and 7, respectively. Finally, the conclusion is presented in Section 8.

2. FC-PHEV description

Fig. 1 represents a serial topology of a FC-PHEV where the fuel cell is not required to follow precisely the dynamics of the driver power demand if the battery pack is well sized. In addition, with this topology, the fuel cell can be optimally set to provide power.

We consider that the sub-system comprising the uni-directional DC–DC converter and the fuel cell represents the fuel cell power source. The driver provides two different signals: the brake and acceleration commands. Given these signals, the Power Demand Module generates the corresponding mechanical power request P_{u} which is further sent to Energy Management System (EMS). P_{u} is interpreted as the desired mechanical power during a trip. In addition, the EMS receives the stored hydrogen energy E_{fc}, the available energy in the battery pack E_{b}, the different power source efficiency maps (not represented in Fig. 1) and the hydrogen/electricity cost ratio (the cost of 1 kW h of hydrogen divided by the cost of 1 kW h of electricity).

Taking into account all this information and considering that the vehicle mass M can vary during the trip, the role of the EMS is to find the most appropriate power splitting of P_{u} by providing the fuel cell optimal reference power command P^*_{fc} and the Propulsion System reference power command P^*_{m}. The fuel cell DC–DC converter is responsible for providing P_{fc} that corresponds to P^*_{fc}. On the other hand, the Propulsion System controller (not represented in Fig. 1) generates the vehicle mechanical power P_{m} using the reference command P^*_{m}. P_{b} represents the battery pack power: a positive value indicates that the battery pack is providing electrical power whilst a negative value indicates that the battery pack is being recharged.

In this paper, we consider the two-layer architecture proposed in Ref. [29] in which the upper layer is responsible of the globally optimal energy profile during the trip whilst the lower layer role is to split the power demand so that the vehicle energy consumption follows this globally optimal profile.

3. FC-PHEV longitudinal model

Assume that the wind speed relative to the ground is negligible. The FC-PHEV longitudinal dynamics is represented by Equation (1) [14] and the corresponding mechanical power is given by (2).

$$F_{\mathrm{m}}(k) = M\dot{v}(k) + \frac{1}{2}\rho_{\mathrm{a}} C_{\mathrm{d}} A v^2(k) + Mg\sin(\theta(k)) + Mg\mu\cos(\theta(k)) \quad (1)$$

where k, F_{m}, M, g, ρ_{a}, μ, C_{d} and A represent respectively the sampling index, the resultant mechanical force, the vehicle's total mass, the gravity constant, the air density, the rolling resistance coefficient, the air drag coefficient and the active frontal area; θ, $\dot{v}$ and v represent respectively the road grade, the longitudinal acceleration and the vehicle speed. $0 < k \leq N$ where N is the number of samples in a given driving cycle.

$$P_{\mathrm{m}}(k) = F_{\mathrm{m}}(k)v(k) \quad (2)$$

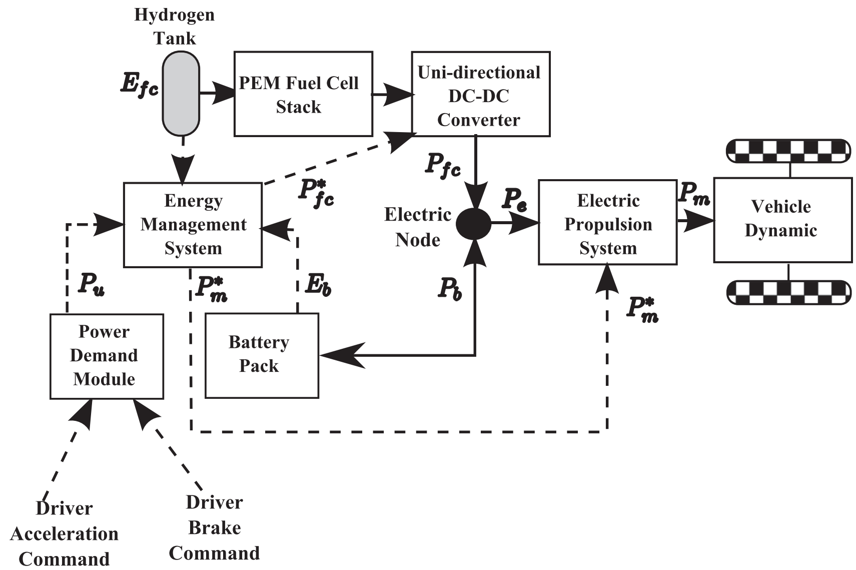

Fig. 1. Fuel cell plugin hybrid electric vehicle: the arrows with the solid lines represent the energy flows; the arrows with the dashed lines indicate the control and measured signals.

The power balance at the electric node (see Fig. 1) is given by Equation (3).

$$P_b(k) = P_e(k) - P_{fc}(k) \tag{3}$$

where P_e is the electric power provided to the powertrain.

Knowing the powertrain efficiency map η_m and the mechanical power at the vehicle wheels, the expression of P_e yields:

$$P_e(k) = \eta_m^{-1}(k) P_m(k) \tag{4}$$

The variation of battery pack energy E_b is represented by the following equation:

$$E_b(k+1) = E_b(k) - \eta_b^{-1}(k) P_b(k) \Delta T \tag{5}$$

where ΔT and η_b represent, the sample time period and the battery pack efficiency, respectively.

Assume that the fuel cell parameters are adequately controlled. The energy balance in the hydrogen tank [30–32] is given by:

$$E_{fc}(k+1) = E_{fc}(k) - K_{H_2} \dot{m}_{H_2}(k) \Delta T \tag{6}$$

where E_{fc}, K_{H_2} and $\dot{m}_{H_2}$ represent the hydrogen energy in the storage, the hydrogen high heating value [33,34] and the hydrogen flow rate, respectively. The fuel cell power system efficiency η_{fc} is defined as:

$$\eta_{fc}(k) = \frac{P_{fc}(k)}{K_{H_2} \dot{m}_{H_2}(k)} \tag{7}$$

To take into account the fuel cell dynamics, the following equation previously proposed in Refs. [29,30,35] is used:

$$P_{fc}(k+1) = A(k) P_{fc}(k) + B(k) P^*_{fc}(k) \tag{8}$$

where $0 \leq A(k) \leq 1$, $B(k)$ and $P^*_{fc}(k)$ represent respectively the Fuel Cell dynamic constant, the input coefficient and the input power command (see Fig. 1). The sequences of A and B can be determined through any classical system identification methods.

4. Energy management system

The FC-PHEV has two energy sources: the battery pack is acting as the primary source and the fuel cell is the secondary source that cannot sustain alone the power demand. For long range operation, the battery pack which is initially fully charged, is unable to provide the total required energy. Instead, the fuel cell supplements the power provided by the primary source. However, the hydrogen cost is generally higher than the electricity from the grid and this cost ratio must be taken into account when designing the Energy Management System.

To allow the battery pack to not being depleted below a given minimum energy threshold, the EMS must determine the appropriate time to start the fuel cell. Indeed, if the fuel cell is started late during the trip, the battery pack energy may drop under this minimum threshold at the end of the trip. On the other hand, as the battery pack is assumed to be initially completely charged, starting too earlier the fuel cell may reduce its capacity to adequately handle the regenerative power source during the trip. Furthermore, the EMS must take into account the fact that the vehicle and load mass can vary during the trip.

The upper layer which is part of the EMS architecture, provides the global and optimal energy consumption profile. The energy profile will therefore be used to estimate the anticipated battery pack depth-of-discharge. In the following section, this layer problem formulation and design are proposed.

4.1. Global energy planning

The first task of the upper layer within the EMS is to estimate the global energy consumption for a given trip by considering only the prescribed speed limit and the position of traffic lights and stop signs. In addition, it must take into account the mass variation. Speed limit and position of traffic lights and stop signs are commonly available for each urban road and highway segment, and are independent of the vehicle driver's behavior [36]. This two

information and the road grade can be also retrieved from any Geographic Information System (GIS) device or any appropriate traffic flow database system.

The speed limit profiles for all road-trip segments may have abrupt changes in the speed values which may produce high accelerations if these profiles are used as driving cycle for a vehicle. These high accelerations are clearly not energetically efficient [37–40]. Hence, the method proposed in Ref. [29], which is based upon the vehicle longitudinal motion (see Equation (1)), will be used to derive the most energy-efficient speed profile for a typical vehicle whilst respecting the trip duration. However, this method depends on M. So the global energy planning is formulated as follows:

Given a road-trip destination, the corresponding road-segment speed limit profiles, the position of traffic light and the road grade, propose an energy-efficient planning by considering that the vehicle mass may vary during the trip.

To solve this problem, we use the upper layer (global energy planning layer) diagram represented in Fig. 2 which will be deeply discussed in next sections. At the beginning of the trip, the planning layer retrieves the destination provided directly by the driver, the default vehicle mass which is considered as the initial mass and the other vehicle physical parameters. With the provided trip destination, each road-segment speed limits and traffic light (or stop signs) position are also retrieved from a GIS. In addition, the road grade profile is obtained from this system and with this information, an energy-efficient driving cycle is computed over the entire trip route. Using the computed driving profile, the electric power, the energy consumptions and the anticipated end-of-trip DoD are deduced and provided to the lower layer which role is to split the driver power demand between the battery pack and the fuel cell.

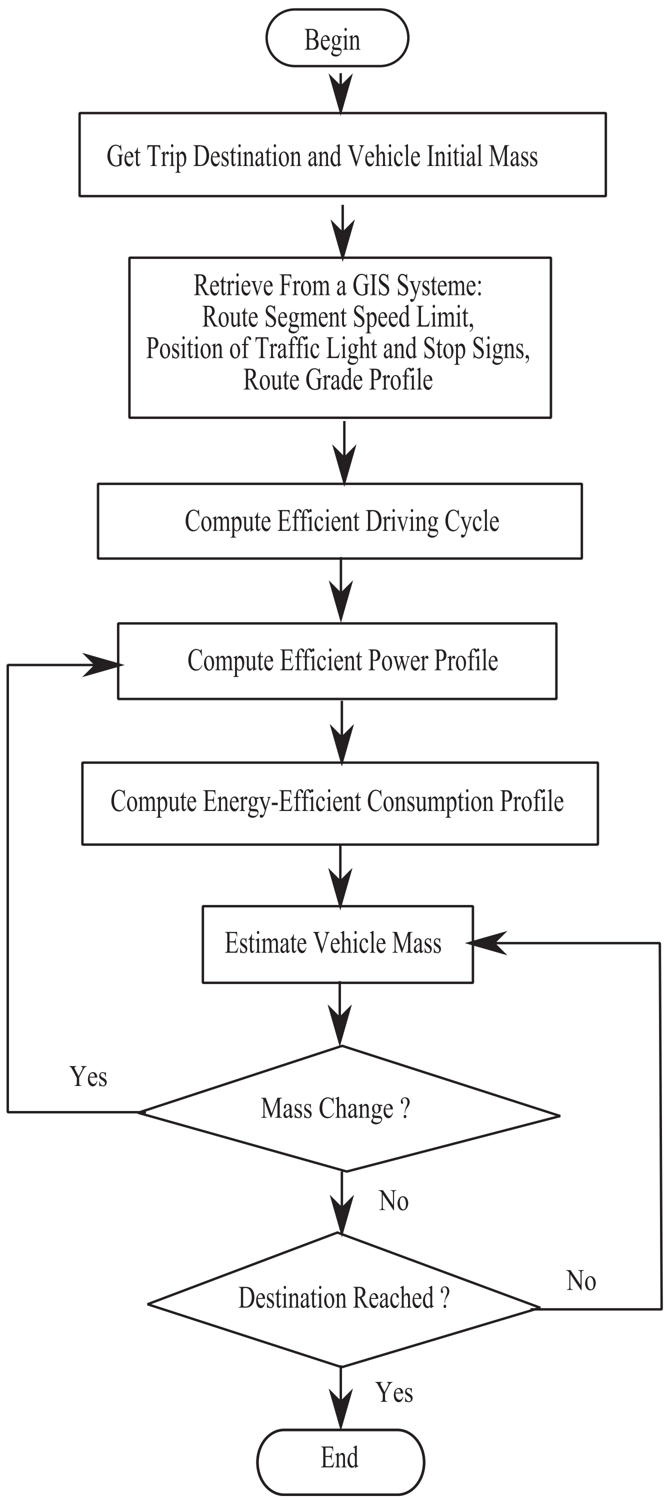

Fig. 2. Global energy planning with varying mass.

4.2. Energy efficient driving cycle

4.2.1. Problem formulation

To find an energy efficient driving cycle, we assume that the vehicle with bounded acceleration/deceleration (real vehicle) is following a vehicle with no limitation (virtual vehicle). Since the virtual vehicle has no limitation, it can follow precisely the speed limit profile $\{v_l(k), k = 1, 2, 3, \ldots, N\}$ retrieved from the GIS. N is the number of samples over the route-trip. The states of the real and virtual vehicles are designated by $X(k) = [x(k), v(k)]^T$ and $X_v(k) = [x_v(k), v_v(k)]^T$, respectively. The dynamic state equations of the two vehicles are represented by Equations (9) and (12), respectively.

$$\begin{bmatrix} x(k+1) \\ v(k+1) \end{bmatrix} = \begin{bmatrix} x(k) + v(k)\Delta T \\ v(k) + u(k)\Delta T - \alpha(k)\Delta T \end{bmatrix} \tag{9}$$

where

$$\alpha(k) = \frac{1}{2\widehat{M}(k)}\rho_a A C_d v^2(k) + g\sin(\theta) + \mu g\cos(\theta) \tag{10}$$

$$u(k) = \frac{F_m(k)}{\widehat{M}(k)} \tag{11}$$

ΔT is the sampling period. $\widehat{M}(k)$ is the estimated vehicle mass at timestamp k. The algorithm for mass estimation is presented in Section 4.4.

$$\begin{bmatrix} x_v(k+1) \\ v_v(k+1) \end{bmatrix} = \begin{bmatrix} x_v(k) + v_v(k)\Delta T \\ v_l(k) \end{bmatrix} \tag{12}$$

Actually, $\{v_l(k), k = 1, 2, 3, \ldots, N\}$ is the worst speed profile from an energetic point of view, as it implies large accelerations and decelerations at the speed limit boundaries. The problem of finding an energy-efficient driving cycle becomes one of selecting a solution of an optimal trajectory tracking problem between the vehicle

under study (real vehicle with physical limitations) and the virtual vehicle by minimizing the following cost function:

$$J_{HL}(0) = J_{HL}(N) + \sum_{k=0}^{N-1}\{J_{HL}(k)\} \tag{13}$$

where

$$J_{HL}(N) = \frac{1}{2}[X(N) - X_v(N)]^T Q(N)[X(N) - X_v(N)] \tag{14}$$

and where

$$J_{HL}(k) = \frac{1}{2}[X(k) - X_v(k)]^T Q(k)[X(k) - X_v(k)] + \frac{1}{2}u^2(k) \tag{15}$$

and where:

$x_v(k+1) = x_v(k) + v_v(k)\Delta T$ is the trajectory obtained when the virtual vehicle is moving along the trip route at the speed limits v_l. $Q \geq 0$ represents the penalty matrix associated with the deviation between X_v and X.

The first term of the cost function (15) will let the real vehicle trajectory be close to the virtual one over the trip route, whereas the second term is introduced to take into account the requirement of low accelerations/decelerations on the real vehicle when tracking the virtual vehicle through the speed limits. These low accelerations/decelerations are one of the key characteristics of an energy-efficient driving cycle.

4.2.2. Optimal state tracking solution

The optimal command sequence $\{u^*(k),\ k = 0,\ldots, N - 1\}$ is defined as [29]:

$$u^* = \arg\min_u J_{HL}(0) \tag{16}$$

with the dynamic constraint represented by Equation (9) and with the following additional nonlinear constraints:

$$u_{min} \leq u(k) \leq u_{max} \tag{17}$$

$$v_{min} \leq v(k) \leq v_{max} \tag{18}$$

where u_{min}, u_{max}, v_{min} and v_{max} represent the allowed real vehicle minimum and maximum commands, minimum and maximum speed values, respectively.

In the present paper, the dynamic programming method has been used to compute the solution $u^*(k)$ [10,41–43]. The optimal state sequence $\{X^*(k) = [x^*(k), v^*(k)]^T,\ k = 0,\ldots, N\}$ is given by:

$$\begin{bmatrix} x^*(k+1) \\ v^*(k+1) \end{bmatrix} = \begin{bmatrix} x^*(k) + v^*(k)\Delta T \\ v^*(k) + u^*(k)\Delta T - \alpha^*(k)\Delta T \end{bmatrix} \tag{19}$$

where $\alpha^*(k) = (1/2\widehat{M}(k))\rho_a A C_d (v^*(k))^2 + g\sin(\theta) + \mu g\cos(\theta)$

The energy-efficient driving cycle is therefore given by the expression of $\{v^*(k),\ k = 1,\ldots, N\}$ from Equation (19).

4.3. Energy-efficient power consumption planning

Using the energy-efficient driving cycle v^* and the optimal command u^*, the corresponding energy-efficient power is given by:

$$P^*_m(k) = \widehat{M}(k)u^*(k)v^*(k) \tag{20}$$

In practice, the driver may not follow exactly the optimal driving cycle. Hence, we must take into account the real mechanical power P_m and the fuel cell power contribution. Knowing the initial energy $E_b(0)$, the optimal battery pack energy profile is given by:

$$\begin{aligned} E^*_b(k+1) = {} & E_b(0) - \sum_{i=1}^{k}\left([\eta_b\eta_m]^{-1}P_m(i) - \eta_b^{-1}P_{fc}\right)\Delta T \\ & - [\eta_b\eta_m]^{-1}P^*_m(k+1)\Delta T \end{aligned} \tag{21}$$

For a given timestamp k, the theoretical battery pack energy at the end of the trip is determined using the following equation:

$$\begin{aligned} E^*_b(N) = {} & E_b(0) - \sum_{i=1}^{k}\left([\eta_b\eta_m]^{-1}P_m(i) - \eta_b^{-1}P_{fc}\right)\Delta T \\ & - \sum_{j=k+1}^{N}\left([\eta_b\eta_m]^{-1}P^*_m(j)\Delta T\right) \end{aligned} \tag{22}$$

It is worth mentioning that $E^*_b(N)$ is directly related to the anticipated battery pack depth-of-discharge. Since it is desirable to not over-discharge the battery pack, a minimum energy E_b^{min} should be kept. In other words, $E^*_b(N) \geq E_b^{min}$. The fuel cell must be operated to avoid violating this condition. One of the lower layer goals is the optimal operation of the fuel cell in order to fulfill to the battery pack minimum energy requirement. This layer detail design is present in section 5.

4.4. Online vehicle mass estimation

To be able to predict the energy consumption accurately, the vehicle mass needs to be estimated. If we assume that the vehicle dynamics is dominated by its longitudinal motion and the road grade is known, the RLS method proposed in Ref. [23] is a good candidate for the vehicle mass estimation. This method can be implemented in real-time and is simple to use in practice. Indeed, the propulsion torque τ_m required during the estimation process is obtained knowing the electric power to mechanical power transformation map η_m:

$$\tau_m(k) = \frac{P_m(k)R_m}{v(k)} \tag{23}$$

where R_m is the wheel radius divided by the total gear ratio and $P_m(k)$ is the mechanical power which can be written as a first order autoregressive model with external input (ARX) and which is deduced, when the vehicle speed $v(k)$ at timestamp k is different to zero, from Equation (4) as follows: [29]

$$P_m(k) = \eta_m(P_e(k), P_m(k-1)) \tag{24}$$

As proposed in Ref. [23] and as we assume that the trip route is known in advance, the route grade $\{\theta(k),\ k = 1, 2,\ldots, N\}$ can be also known. Therefore, the dynamic Equation (1) is rewritten as follows:

$$\begin{aligned} M\dot{v}(k) = {} & \frac{(\tau_m - J_m\dot{\omega}_m)}{R_m} - \frac{1}{2}\rho_a C_d A v^2(k) - Mg\sin(\theta(k)) \\ & - Mg\mu\cos(\theta(k)) \end{aligned} \tag{25}$$

where J_m, $\dot{\omega}_m$ represent the powertrain inertia, the powertrain rotation acceleration, respectively. J_m and R_m are provided by the vehicle manufacture.

From Equation (25), the vehicle net acceleration $\dot{v}$ is:

$$\begin{aligned} \dot{v}(k) = {} & \frac{1}{M}\left(\frac{(\tau_m - J_m\dot{\omega}_m)}{R_m} - \frac{1}{2}\rho_a C_d A v^2(k)\right) - g\sin(\theta(k)) \\ & - g\mu\cos(\theta(k)) \end{aligned} \tag{26}$$

Rewriting Equation (26) yields the following linear parametric expression in which the unknown parameter M can be

estimated using the well-known recursive least squares (RLS) algorithm:

$$O(k) = \beta(k)\phi(k) \tag{27}$$

where the observation sequence $O(k)$, $k = 1, 2, \ldots, N$ (N is the number of samples) is represented by:

$$O(k) = \dot{v}(k) + g\sin(\theta(k)) + g\mu\cos(\theta(k)) \tag{28}$$

and where the regressor $\phi(k)$ is represented by:

$$\phi(k) = \left(\frac{(\tau_{\mathrm{m}} - J_{\mathrm{m}}\dot{\omega}_{\mathrm{m}})}{R_{\mathrm{m}}} - \frac{1}{2}\rho_a C_d A v^2(k)\right) \tag{29}$$

and where the parameter to be identified is:

$$\beta(k) = \frac{1}{M} \tag{30}$$

The estimated mass $\widehat{M}$ is deduced from the recursive estimation $\widehat{\beta}$ of β.

5. Cost effective power splitting

In this section, we present the detail design of the lower layer which is responsible for the power demand splitting between the fuel cell and the battery pack. At each timestamp during the trip, the upper layer provides the anticipated final energy $E_b(N)$ in the battery pack (see Equation (22)). This value is used to compute the DoD. The first requirement for the lower layer is to keep the final energy $E_{\mathrm{b}}(N)$ greater than $E_{\mathrm{b}}^{\mathrm{min}}$. In addition, it should take into account some desirable criteria:

1. Always operate the fuel cell at its maximum efficiency in order to minimize hydrogen consumption.
2. Energy cost: since the energy cost in battery may be different with hydrogen cost, the splitting method must reduce the total energy usage cost.
3. Driving power compliance: the splitting method must let the vehicle mechanical power to be close to the power demand in order to give to the driver, the feeling that he is actively controlling the vehicle dynamics.

One way to integrate these criteria when designing the lower layer power splitting method is to formulate and solve an optimal control problem.

5.1. Optimal power splitting problem formulation

For each timestamp k, let's define a fuel cell power reference profile $P_{\mathrm{fc}}^{\mathrm{r}}(k)$ based on power hysteresis function as shown in Fig. 3:

- $P_{\mathrm{fc}}^{\mathrm{r}}(k) = P_{\mathrm{fc}}^{\mathrm{max}}$ if $E_{\mathrm{b}}^{*}(N) \le E_{\mathrm{b}}^{\mathrm{min}}$
- $P_{\mathrm{fc}}^{\mathrm{r}}(k) = 0$ if $E_{\mathrm{b}}^{*}(N) > E_{\mathrm{b}}^{\mathrm{max}}$
- $P_{\mathrm{fc}}^{\mathrm{r}}(k) = P_{\mathrm{fc}}^{\mathrm{r}}(k-1)$ if $E_{\mathrm{b}}^{\mathrm{min}} \le E_{\mathrm{b}}^{*}(N) \le E_{\mathrm{b}}^{\mathrm{max}}$

where $P_{\mathrm{fc}}^{\mathrm{max}}$ is the fuel cell power production at maximum efficiency.

Minimizing the following cost function could provide a good trade-off for the splitting method:

$$J_{\mathrm{LL}}(k) = \frac{1}{2}\left\{\left(P_{\mathrm{fc}}(k) - P_{\mathrm{fc}}^{\mathrm{r}}(k)\right)^2 + CP_{\mathrm{fc}}^2(k) + (P_{\mathrm{m}}(k) - P_{\mathrm{u}}(k))^2\right\} \tag{31}$$

where C represents the cost ratio defined as the ratio between hydrogen and grid electricity costs.

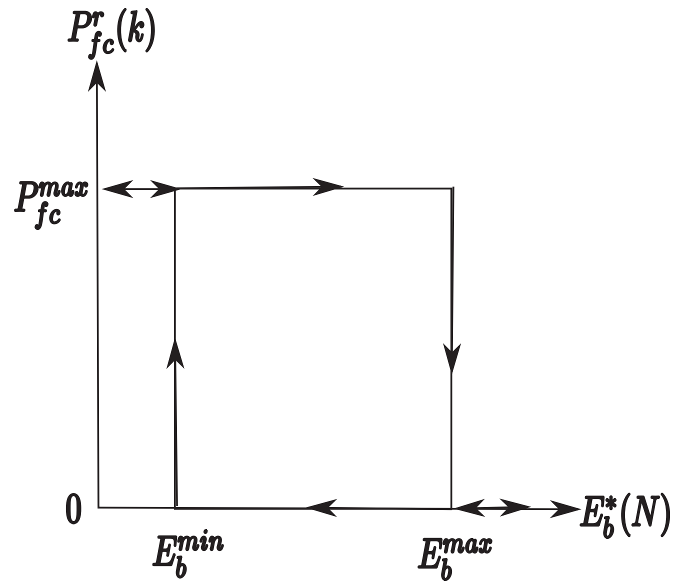

Fig. 3. Power hysteresis function.

The first term of J_{LL} is added in order to take into account the minimum battery energy requirement. Indeed, if the upper layer anticipates that $E_{\mathrm{b}}(N)$ will be less than $E_{\mathrm{b}}^{\mathrm{min}}$, $P_{\mathrm{fc}}^{\mathrm{r}}$ will be equal to $P_{\mathrm{fc}}^{\mathrm{max}}$ and the only way to minimize $(P_{\mathrm{fc}}(k) - P_{\mathrm{fc}}^{\mathrm{r}}(k))^2$ is set the fuel cell to operate close to its maximum power. The second term takes into account the energy cost ratio and will be minimized if $P_{\mathrm{fc}} = 0$. Finally, the third term is used for power compliance. Indeed, if the powertrain mechanical power P_{m} is closed to the driver power demand P_{u}, this term is minimized.

5.2. Real-time power splitting solution

To allow the design of a simple, practical and real-time solution, we propose the following power splitting algorithm which provides the local optimal control signals for the fuel cell P_{fc}^{*} and the powertrain P_{m}^{*}:

- set P_{m}^{*} to P_{u}: therefore, the third term is minimized.
- since the fuel cell power $P_{\mathrm{fc}}^{\mathrm{r}}$ can take only two different values (0 and $P_{\mathrm{fc}}^{\mathrm{max}}$), use each of them to evaluate J_{LL}.
- select the fuel cell power that gives the minimum value of J_{LL}.
- set P_{fc}^{*} to that value.

6. Validation using experimental data

Since the energy planning layer is independent on the way the power is splitted by the lower layer, we propose to validate the following aspects pertaining to this layer:

- the offline optimal driving cycle calculation using dynamic programming and GIS data;

Table 1
Vehicle parameters.

Parameter	Value	Parameter	Value
M	986 kg (default value)	A	2.3 m^2
ρ_a	1.22 kg m^{-3}	μ	0.018
C_d	0.7	θ, $\forall k$	0 rad
$u_{\max}$	4 m s^{-2}	$u_{\min}$	−2 m s^{-2}

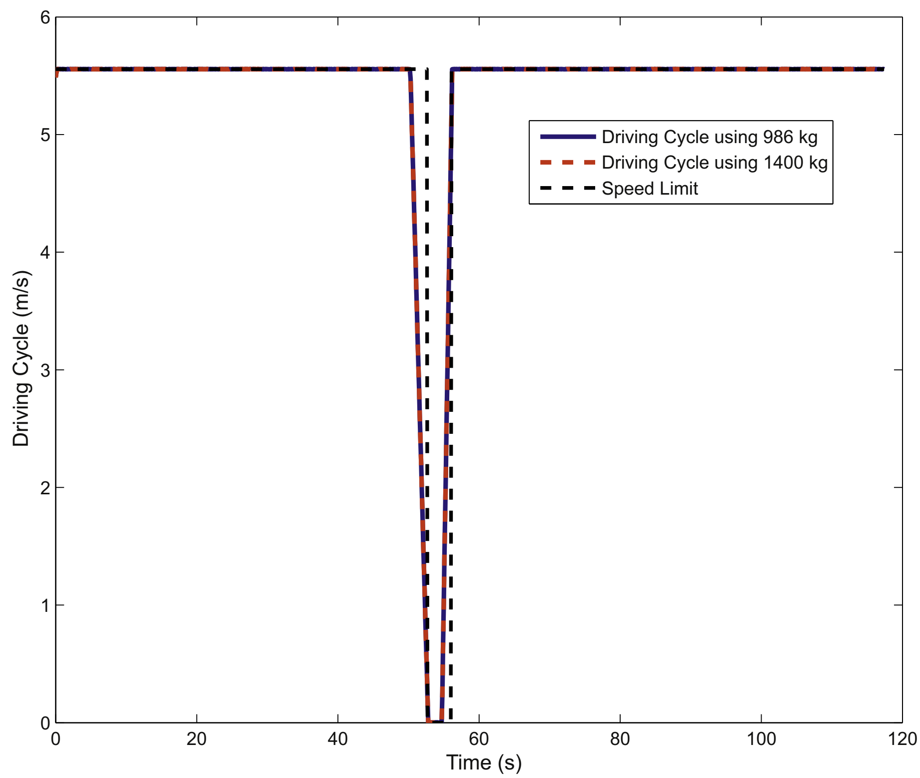

Fig. 4. Driving cycles comparison.

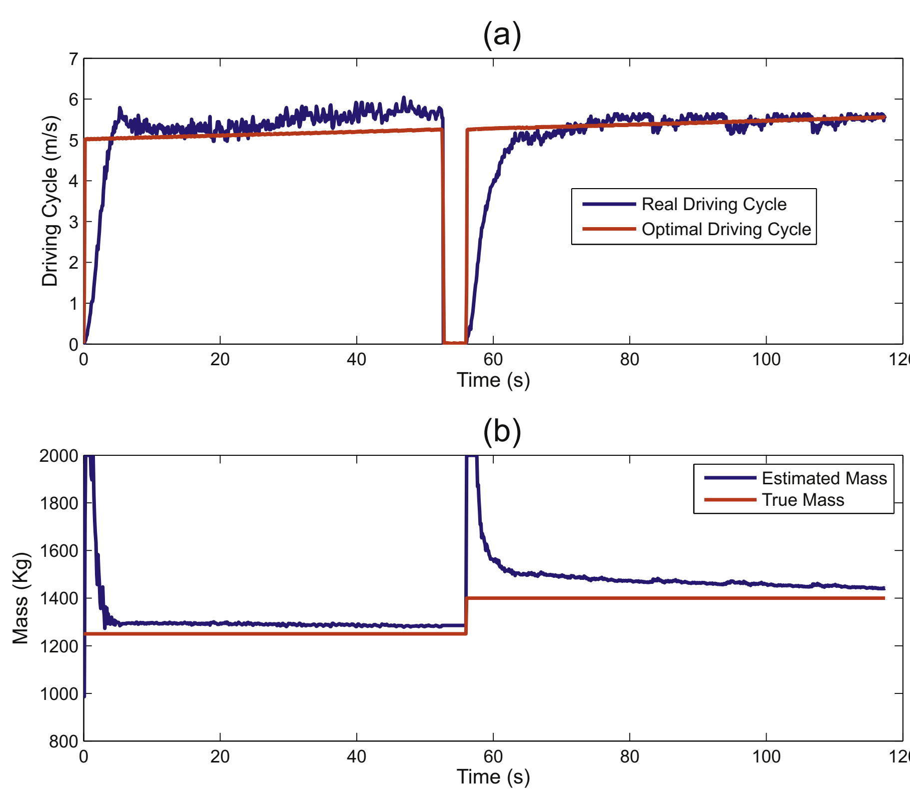

Fig. 5. Driving cycles and mass: (a) experimental driving cycle (blue curve) and optimal driving cycle using road segment speed limits (red curve). (b) True mass (red curve) and estimated mass using RLS algorithm (blue curve). (For interpretation of the references to color in this figure legend, the reader is referred to the web version of this article.)

- the online vehicle mass estimation using the consumed electric power, the produced mechanical power and the RLS.

In addition, the advantages of adapting energy planning method with the mass estimation is shown through a comparative study.

6.1. Experimental scenario

A small truck (maximum speed 40 Km h^{-1}) equipped with a lead-acid battery pack (rated to 72 V, 180 Ah) and a fuel cell system (1.5 kW) is used for experiments. The sampling frequency is set to 10 Hz. The vehicle physical parameters are summarized in Table 1. One can notice that the vehicle mass provided by the manufacturer is 986 kg (default value). However, in our test scenario, the truck mass at the beginning of the experiment is measured, and it was found that the value is 1250 kg.

During the experiment, the truck moved on a flat road (with a 0 grade value) and the driver was instructed not to exceed the speed limit of 20 km h^{-1} (5.56 m s^{-1}). Between $k = 51$ s and $k = 56$ s, the truck is stopped and a load of 150 kg added. Then, its started moving again on this flat road upto $k = 117$ s.

6.2. Optimal driving cycle validation

Since the dynamic programming is a time-consuming process, the first task is to evaluate the impact of the varying mass on the optimal driving cycle. So two driving cycles were computed: the vehicle default mass is used for the first one whereas a 1400 kg is used for the second one.

Fig. 4 shows the speed limit, the driving cycle if the vehicle mass is 986 kg (default mass value) and the driving cycle obtained when the vehicle mass is 1400 kg. The speed limit profile (dashed curve) has sharp value changes at $k = 51$ s and $k = 56$ s. The optimal driving cycles obtained with each of the two masses are similar (the blue curve (in the web version) is similar to the red one). The relatively small root mean squared error (0.0015) indicates that the two curves are very close to each other. This result suggests that at low speed, the optimal driving cycle is little sensitive to the varying mass. Therefore, using the default mass value, the optimal driving cycle is computed offline once. On the other hand, the energy consumption is dynamically updated with the vehicle mass estimation. At high speed, the optimal driving cycle may be sensitive to the vehicle total mass. In this, the optimal driving cycle could be computed offline (with dynamic programming) for the worst-case scenario using the maximum allowed mass.

6.3. Online mass estimation validation

Three different mass values are involved in the experiment: the default mass (986 kg), the mass at the beginning of the experiment (1250 kg) and the mass after $k = 56$ s (1400 kg). The high level layer knows only the default mass value before the vehicle started moving. The vehicle speed v and the electric power consumption P_e are monitored at each timestamp k. The power transformation map $\eta_m(k) = P_m(k)/P_e(k)$ has been estimated using the following empirical expression [29]:

$$\eta_m(k) = 0.57 P_m(k-1) P_e^{-1}(k) + 0.2176, \; P_e(k) \neq 0 \tag{32}$$

Using the estimation presented in section 4.4, the vehicle mass is iteratively evaluated as followed:

- With the measured value of $P_e(k)$ and using Equation (24), the mechanical power $P_m(k)$ is estimated.
- The estimated $P_m(k)$ and the speed $v(k)$ is used to deduce the torque $\tau_m(k)$ (see Equation (23)).
- Knowing J_m and $\dot{\omega}_m$, the RLS algorithm is applied to find the estimation $\hat{M}$ of the vehicle mass M.

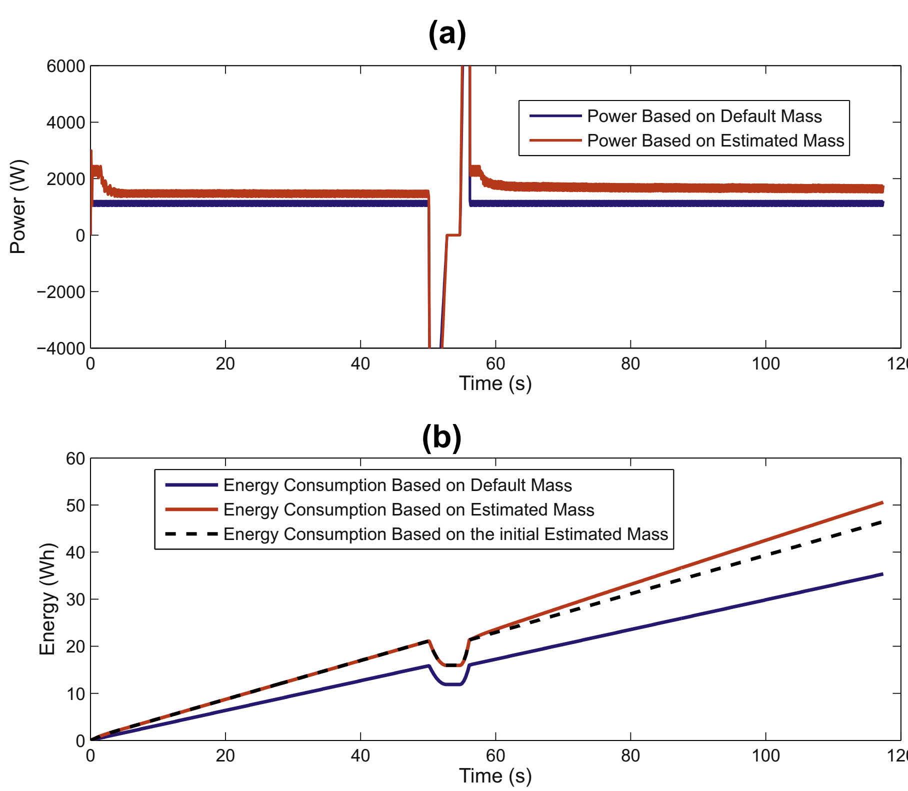

Fig. 6. Power and energy profiles: (a) power profile; (b) energy profile.

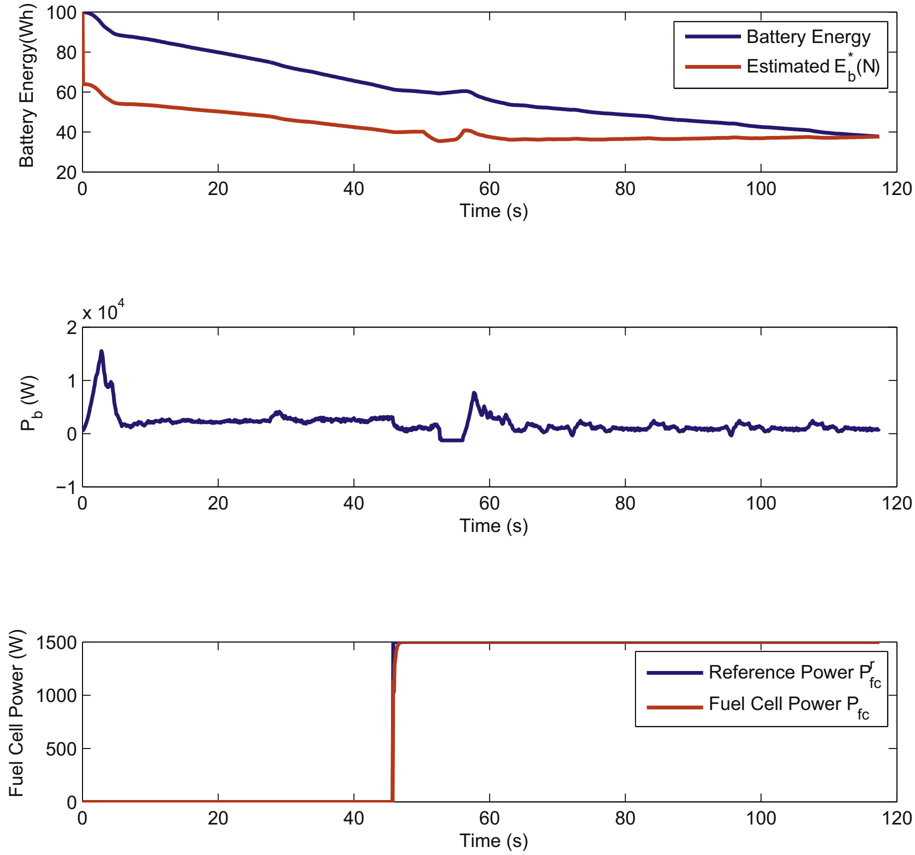

Fig. 7. Power splitting with the default vehicle mass.

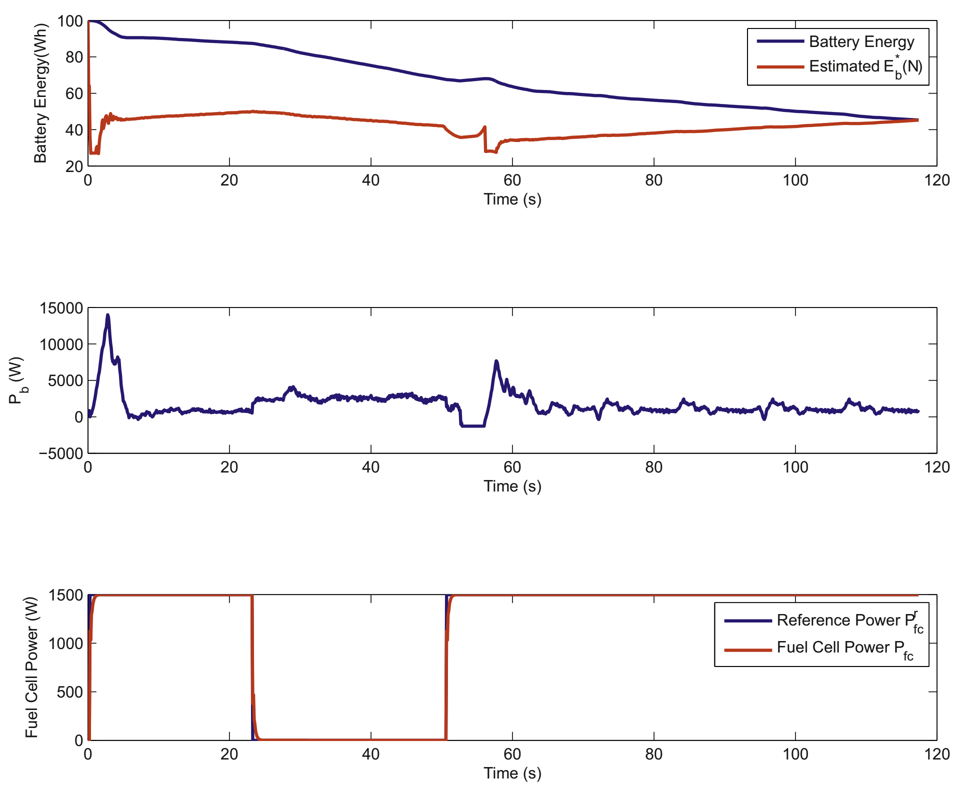

Fig. 8. Power splitting with adaptive vehicle mass.

Fig. 5, shows the mass estimation results. The vehicle speed (blue curve) and the optimal driving cycle (red curve) are represented on the graph (a) of this figure. On the graph (b) is shown the estimated mass during the vehicle motion and the true mass. Although the default mass of 986 kg is different with the initial mass, one can observe that $\widehat{M}$ converges quickly towards 1250 kg which is the true mass for $k < 56$ s. After the mass has been changed ($k > 56$ s), the estimation algorithm converges towards 1400 kg which is the true mass. Thus, the proposed iterative estimation method provides satisfactory results.

6.4. Effect of adapting energy planning with estimated mass

As shown in Fig. 2, we use the estimated mass to dynamically update the planned power usage as well as the corresponding energy consumption and the end-of-trip DoD. These two profiles are presented in Fig. 6 where we compared the power and the energy profiles by considering the vehicle default and estimated mass. On graph (a), we observe that there is a significant difference between the power obtained using the default mass value (blue curve (in the web version)) and the one with the estimates mass (red curve). This difference is the main reason of the under estimated energy consumption with the default mass value (blue curve of graph (b)). In addition, we showed on graph (b) that estimating the mass only once at the beginning of the trip is not enough to predict the vehicle energy consumption. Indeed, in our test scenario, the initial mass is 1250 kg and the dashed line on graph (b) indicates the energy profile by considering this mass for the whole trip. Clearly, a significant difference exists between that energy profile and the profile with the estimated mass. This result indicates that a good mass estimation is required to properly plan the vehicle energy consumption for a given trip.

7. Power splitting method validation

This section aims at providing evidence that using adaptive mass estimation improves the hybrid vehicle energy management system and the associated power splitting method. We used the scenarios described in Section 6.1 to validate the power splitting method and the whole energy management system. The following parameters are used: $P_{fc}^{max} = 1500$ W, $E_b(0) = 100$ Wh, $E_b^{min} = 40$ Wh, $E_b^{max} = 50$ Wh.

Two tests are performed: in the first test, we compared the battery pack (DoD) when the proposed power splitting method is used with and without adaptive mass estimation. The DoD is defined as:

$$\mathrm{DoD}(k) = \frac{E_b(0) - E_b(k)}{E_b(0)} \tag{33}$$

The second test is related to the analysis of the impact of the hydrogen/electricity cost ratio on the battery DoD with adaptive mass estimation.

7.1. Mass estimation impact on power splitting

The cost ratio C is set to 1 meaning that the hydrogen and grid electricity costs are similar. In addition, the fuel cell is supposed to be stopped at the beginning of the trip. Fig. 7 shows the result when the default mass (986 kg) is used with the power splitting method. On graph (a), the estimated battery end-of-trip energy at the ($E_b^*(N)$) using the default known mass (red curve) becomes less than $E_b^{min} = 40$ Wh at $k > 45.7$ s. So the power reference profile $P_{fc}^r(k)$ changed from 0 to P_{fc}^{max} and the fuel cell was started until the end of the trip (see graph (c)). Although the fuel cell contributes to provide energy,

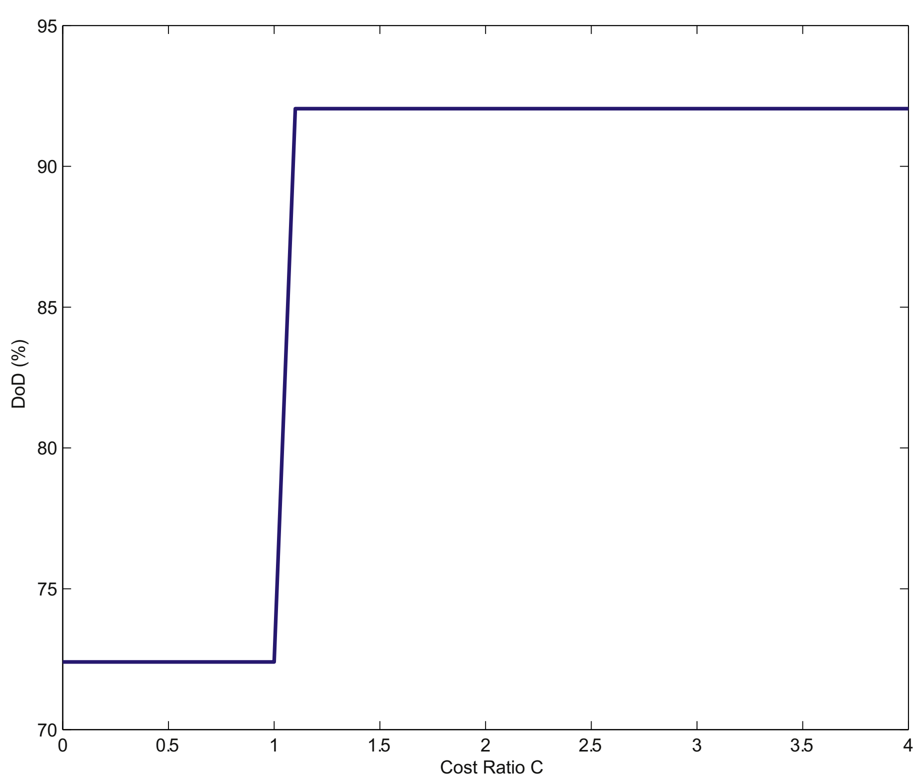

Fig. 9. DoD as a function of the cost ratio.

$E_b^*(N) = 38.71$ Wh which is less than $E_b^{min} = 40$ Wh. The end-of-trip DoD is estimated to 61.29%.

Using the adaptive mass estimation during the trip (1250 kg and 1400 kg), Fig. 8 shows that the estimated battery energy at the end of the trip ($E_b^*(N)$) has reached the minimum value (E_b^{min}) in two times and so the fuel cell was started twice: from $k = 1$ to $k = 23.2$ s and from $k = 50.9$ s to $k = 117.4$ s. The estimated end-of-trip battery energy is 45.24 Wh which is greater than E_b^{min}. Hence the minimum battery energy is not violated with the adaptive splitting method. Furthermore, the corresponding DoD value is 54.76% which is greater than the DoD value obtained with the default mass. This DoD improvement has a positive impact on the battery pack degradation and efficiency.

7.2. Fuel cost impact on power splitting

We consider that the vehicle mass is continuously estimated. To analyze the impact of the energy cost ratio on the DoD, we run several tests in which C value varies from 0.1 (hydrogen is much cheaper than electricity) to 4 (hydrogen is much more expensive than electricity). Fig. 9 shows the DoD as a function of C. One can observe that as the cost ratio is less or equal to 1 (hydrogen is less or as expensive as electricity), the splitting method allows the fuel cell to contribute to vehicle traction power. Indeed, from Equation (32), by setting $P_m = P_u$, $J_{LL}(k)$ becomes: $J_{LL}(k) = 1/2\{(P_{fc}(k) - P_{fc}^r(k))^2 + CP_{fc}^2(k)\}$. The relative weight of P_{fc}^2 is less than the weight of $(P_{fc}(k) - P_{fc}^r(k))^2$. One way to minimize J_{LL} is to let P_{fc} to follow P_{fc}^r. On the other hand, if C is greater than 1 meaning that hydrogen is more expensive than electricity, the relative weight of $(P_{fc}(k) - P_{fc}^r(k))^2$ is less than the weight of P_{fc}^2. So to minimize J_{LL}, the splitting method sets P_{fc} to 0. Therefore, no hydrogen is used.

8. Conclusion

We proposed an adaptive energy management and power splitting method for fuel cell hybrid electric vehicle. This method is based on a two layer architecture in which the upper one is responsible for estimating the battery pack depth-of-discharge using the online mass evaluation. Given the estimated depth-of-discharge, the lower layer uses an optimal power splitting algorithm to share the power demand between the fuel cell and the battery pack. The goal of this splitting algorithm is to improve the depth-of-discharge while taking into account the cost ratio hydrogen/electricity. In addition, the fuel cell is powered on to always work at its maximum efficiency. A comparative study demonstrated that by taking into account the online mass estimation, the overall energetic efficiency is improved.

Acknowledgment

This work was supported by "Bureau de l'efficacité et de l'innovation énergétiques, Ministère des Ressources naturelles et de la Faune du Québec" and Natural Science and Engineering Research Council of Canada.

References

[1] P. Poudenx, Transp. Res. Part A Policy Pract. 42 (2008) 901–909.
[2] S. Wirasingha, A. Emadi, IEEE Trans. Veh. Technol. 60 (2011) 111–122.
[3] Z. Amjadi, S. Williamson, in: Electrical Power Energy Conference (EPEC), IEEE, 2009, pp. 1–7.
[4] C. Norman, N. Kaushal, C. Hendrickson, S. Peterson, J. Whitacre, J. Michalek, J. Mech. Des. Trans. ASME 132 (2010) 1–11.
[5] D. Feroldi, M. Serra, J. Riera, IEEE Trans. Veh. Technol. 58 (2009) 4720–4729.
[6] R. Moore, K. Hauer, D. Friedman, J. Cunningham, P. Badrinarayanan, S. Ramaswamy, A. Eggert, J. Power Sources 141 (2005) 272–285.
[7] A. Ferreira, J. Pomilio, G. Spiazzi, L. de Araujo Silva, IEEE Trans. Power Electron. 23 (2008) 107–115.
[8] X. Li, J. Li, L. Xu, M. Ouyang, in: Vehicle Power and Propulsion Conference, IEEE, 2009, pp. 1749–1754. VPPC '09.
[9] M. Kazmierkowski, IEEE Ind. Electron. Mag. 4 (2010) 75.
[10] A. Sciarretta, L. Guzzella, IEEE Control Syst. 27 (2007) 60–70.
[11] G. Wang, P. Yang, J. Zhang, in: International Conference on Intelligent Control and Information Processing (ICICIP), 2010, pp. 555–560.
[12] K. Ettihir, L. Boulon, K. Agbossou, S. Kelouwani, M. Hammoudi, in: IEEE International Symposium on Industrial Electronics (ISIE), 2012, pp. 1714–1719.
[13] Z. Yu, D. Zinger, A. Bose, J. Power Sources 196 (2011/02/15) 2351–2359.
[14] S. Kelouwani, K. Agbossou, Y. Dubé, L. Boulon, J. Power Sources (2012).
[15] S. Kermani, R. Trigui, S. Delprat, B. Jeanneret, T. Guerra, IEEE Trans. Veh. Technol. 60 (2011) 782–792.
[16] P. Pisu, G. Rizzoni, IEEE Trans. Control Syst. Technol. 15 (2007) 506–518.
[17] N. Kim, S. Cha, H. Peng, IEEE Trans. Control Syst. Technol. 19 (2011) 1279–1287.
[18] H. Fathy, D. Kang, J. Stein, in: American Control Conference, IEEE, 2008, pp. 1842–1848.
[19] R. Rajamani, J. Hedrick, IEEE Trans. Control Syst. Technol. 3 (1995) 86–93.
[20] L. Tong, (2012) 56–63.
[21] T. Ghotikar, Estimation of Vehicle Mass and Road Grade. Ph.D. thesis, 2008.
[22] M. McIntyre, T. Ghotikar, A. Vahidi, X. Song, D. Dawson, IEEE Trans. Veh. Technol. 58 (2009) 3177–3185.
[23] A. Vahidi, A. Stefanopoulou, H. Peng, Veh. Syst. Dyn. 43 (2005) 31–55.
[24] V. Winstead, I. Kolmanovsky. CCA 2005, in: Proceedings of 2005 IEEE Conference on Control Applications, IEEE, 2005, pp. 1588–1593.
[25] H. Bae, J. Ryu, J. Gerdes, in: IEEE Conference on Intelligent Transportation Systems, Proceedings, ITSC, pp. 166–171.
[26] A. Vahidi, M. Druzhinina, A. Stefanopoulou, H. Peng, in: Proceedings of the 2003 American Control Conference, vol. 6, IEEE, 2003, pp. 4951–4956.
[27] A. Vahidi, A. Stefanopoulou, H. Peng, in: Proceedings of the ASME International Mechanical Engineering Congress and Exposition, pp. 4951–4956.
[28] M. Mahyuddin, J. Na, G. Herrmann, X. Ren, P. Barber, in: UKACC International Conference on Control (CONTROL), IEEE, 2012, pp. 102–107.
[29] S. Kelouwani, N. Henao, K. Agbossou, Y. Dube, L. Boulon, IEEE Trans. Veh. Technol. 61 (2012) 3851–3864.
[30] A. Arce, A.J. Del Real, C. Bordons, D.R. Ramirez, IEEE Trans. Ind. Electron. 57 (2010) 1892–1905.
[31] R. Methekar, S. Patwardhan, R. Gudi, V. Prasad, J. Process Control 20 (2010/01/) 73–82.
[32] N. Bizon, Appl. Energy 87 (2010) 3115–3130.
[33] A. del Real, A. Arce, C. Bordons, J. Power Sources 173 (2007/11/08) 310–324.
[34] K. Adegnon, Y. Dube, K. Agbossou, in: 2009 Canadian Conference on Electrical and Computer Engineering (CCECE 2009), 2009, pp. 716–719.
[35] S. Kelouwani, K. Adegnon, K. Agbossou, Y. Dubé, IEEE Trans. Energy Convers. 27 (2012a) 580–592 cited by (since 1996) 2.
[36] S. Kelouwani, K. Agbossou, Y. Dubé, L. Boulon, in: IEEE Vehicular Technology Conference (VTC Fall), IEEE, 2012, pp. 1–5.
[37] M. Barth, S. Mandava, K. Boriboonsomsin, H. Xia, in: IEEE Forum on Integrated and Sustainable Transportation System (FISTS), 2011, pp. 182–188.
[38] M. Kamal, M. Mukai, J. Murata, T. Kawabe, in: IEEE International Conference on Control Applications (CCA), 2010, pp. 1636–1641.
[39] M.A.S. Kamal, M. Mukai, J. Murata, T. Kawabe, IEEE Trans. Intell. Transp. Syst. 12 (2011) 783–794.
[40] I. Ben Dhaou, in: Intelligent Vehicles Symposium (IV), IEEE, 2011, pp. 37–42.
[41] J. Kessels, M. Koot, P. van den Bosch, D. Kok, IEEE Trans. Veh. Technol. 57 (2008) 3428–3440.
[42] C.-C. Lin, H. Peng, J. Grizzle, J.-M. Kang, IEEE Trans. Control Syst. Technol. 11 (2003) 839–849.
[43] M. Koot, J. Kessels, B. de Jager, W. Heemels, P. van den Bosch, M. Steinbuch, IEEE Trans. Veh. Technol. 54 (2005) 771–782.